Fusion cross sections of ^{8}B + ^{28}Si at near-barrier energies

A. Pakou,[1] E. Stiliaris,[2] D. Pierroutsakou,[3] N. Alamanos,[4] A. Boiano,[3] C. Boiano,[5] D. Filipescu,[6] T. Glodariu,[6] J. Grebosz,[7] A. Guglielmetti,[5] M. La Commara,[8] M. Mazzocco,[9] C. Parascandolo,[9] K. Rusek,[10] A. M. Sánchez-Benítez,[11] C. Signorini,[9] O. Sgouros,[1] F. Soramel,[9] V. Soukeras,[1] E. Strano,[9] L. Stroe,[6] N. Toniolo,[12] D. Torresi,[9] and K. Zerva[1]

[1]*Department of Physics and HINP, The University of Ioannina, 45110 Ioannina, Greece*
[2]*Institute of Accelerating Systems and Applications and Department of Physics, University of Athens, Athens, Greece*
[3]*INFN – Sezione di Napoli, via Cinthia, I-80126 Napoli, Italy*
[4]*CEA-Saclay, DAPNIA-SPhN, Gif-sur-Yvette, France*
[5]*Universita' degli Studi di Milano and INFN – Sezione di Milano, via Celoria 16, I-20133 Milano, Italy*
[6]*"Horia Hulubei" National Institute of Physics and Nuclear Engineering, Bucharest-Magurele, Romania*
[7]*IFJ-PAN, Krakow, Poland*
[8]*Dipartimento di Scienze Fisiche and INFN – Sezione di Napoli, via Cinthia, I-80126 Napoli, Italy*
[9]*Dipartimento di Fisica and INFN – Sezione di Padova, via F. Marzolo 8, I-35131 Padova, Italy*
[10]*Heavy Ion Laboratory, University of Warsaw, Pasteura 5a, 02-093 Warsaw, Poland*
[11]*Departamento de Física Aplicada, Universidad de Huelva, E-21071 Huelva, Spain*
[12]*INFN – Sezione di Padova, Padova, Italy*

(Received 12 November 2012; revised manuscript received 9 January 2013; published 28 January 2013)

Fusion cross sections were measured for ^{8}B + ^{28}Si at near-barrier energies by detecting the alpha particles produced in the evaporation process. The results present a small suppression with respect to one-barrier penetration model predictions, which could be attributed to incomplete fusion processes and do not differ appreciably from fusion cross sections obtained with weakly bound but stable projectiles on the same target. Comprehensive comparisons of fusion cross sections at sub- and near-barrier energies with various light weakly bound projectiles support a simple tunneling probability with slight modifications due to coupled-channel effects.

DOI: 10.1103/PhysRevC.87.014619 PACS number(s): 25.60.Pj, 25.70.−z

I. INTRODUCTION

Fusion of two nuclei can in principle be understood as a quantum tunneling effect of two structureless objects in a potential depending only on the distance between their centers [1]. Under this scenario it can be described by one-barrier penetration models (BPM) [2]. However, at near-barrier energies and for complex nuclei, the influence of static and dynamic effects, relevant to the detailed structure of both projectile and target nuclei [3] and the reaction mechanisms involved [4], strongly alter this image, and fusion cross sections below and near barrier energies can be interpreted via coupled-channel formalisms [5,6]. It is expected that for exotic nuclei the influence of a neutron (proton) halo or skin will enrich our knowledge relevant to the structure and reaction mechanisms [7–11] but also will lead to the appropriate evidence for producing drip-line nuclei and superheavy elements. While our knowledge on fusion with neutron-rich light projectiles starts to build up [12–18], studies with proton-rich nuclei are scarce. Only one fusion measurement at sub-barrier energies on ^{8}B + ^{58}Ni was recently reported [19].

^{8}B is a proton drip-line beta-decaying nucleus, attracting strong interest due to its role in the production of high-energy neutrinos in the sun [20–23] and its unusual structure with a possible proton halo [24,25]. The last issue is still in an exploratory stage since the Coulomb force may prevent the growth of the halo at distances out of the Coulomb radius. Therefore it is interesting to test the behavior of this nucleus in a fusion process and compare it with that presented by other weakly bound nuclei on various targets. It should be noted that the first fusion measurement reported for both sub- and near-barrier energies [19] very large fusion cross sections, compatible with a BPM prediction only after an elongation of the interaction radius by ∼26%. This experimental finding should be confronted also for other targets.

In general, studies with ^{8}B are scarce, as this beam is produced in flight only in a few laboratories and with low intensities. Therefore special tools had to be invoked to perform a fusion measurement. Adopting the idea of total reaction cross-section measurements, where a silicon detector is used as an active target and the detector itself acts as a calorimeter, we have proceeded with a fusion measurement of ^{8}B + ^{28}Si at near-barrier energies between 20 and 35 MeV. This type of technique was developed by Warner and collaborators [26–28] for total reaction cross-section measurements but it was applied mainly for intermediate energies for stable and exotic nuclei [29–33]. Very recently it was adopted for near-barrier energies with lithium projectiles [34,35]. The results were promising and gave the boost for applications with radioactive beams.

The present fusion measurement is based on the assumption that, during the collision of ^{8}B with silicon, neither the breakup nor a transfer process can produce alpha particles, but an evaporation process can. The transfer of three protons and a neutron to silicon is considered highly improbable, and in any case the high Q value of the reaction ($Q = 12.3$ MeV) guarantees the discrimination between alphas from transfer and alphas from fusion. A transfer of a deuteron with $Q =$ 3.26 MeV leads to ^{6}Be which in turn could give alphas with energies overlapping the fusion ones. However, according to preliminary calculations this probability is very small, and the

contamination could be less than 3%. By using a stack of three detectors instead of one, the discrimination of alpha particles from other reaction events was possible via a conventional ΔE-E technique, which also prevented any contribution from frame scattering, a usual problem in this type of measurements. For the pileup rejection, special techniques were adopted and will be described. In Sec. II we present the experimental technique and the beam production; in Sec. III, the data reduction and the cross-section determination; in Sec. VI, coupled-channel calculations; while in Sec. V, we present comparisons with other weakly bound nuclei and the relevant discussion.

II. EXPERIMENTAL DETAILS

A. Secondary beam

The ^{8}B secondary beam was produced at the EXOTIC facility [36] at Laboratori Nazionale di Legnaro (LNL-Italy) of the Istituto Nazionale di Fisica Nucleare by means of the in-flight (IF) technique and the reaction ^{3}He(^{6}Li,^{8}B)n ($Q = -1.97$ MeV). The ^{6}Li^{+3} primary beam was delivered from the LNL-XTU Tandem Van de Graaf accelerator with intensity of $\sim$150 pnA and at the energies of 42.6 and 49.4 MeV. The primary beam was directed to a 5 cm long gas cell with 2.2 μm thick Havar foils, filled with ^{3}He at a pressure of 1 bar at temperature of 90 K corresponding to an effective thickness of 2 mg/cm^{2}.

The selection, separation, and focusing of the secondary beam were achieved by a quadrupole triplet, a 30° bending magnet, a 1 m long Wien filter and a second quadrupole triplet. Downwards across the beam line and 88 cm before the secondary target was set one parallel plate avalanche counter (PPAC$_A$) and at 35 cm a second one (PPAC$_B$), which were used as to improve and monitor the beam spatial profile before and during the measurement. The beam spatial profile at the target position was defined from an appropriate sequence of slits and collimators with a minimum aperture of 12 mm, in a configuration identical with the one described in Ref. [37]. The beam spot at the target position as determined from the beam reconstruction with the aid of the two PPAC detectors was estimated to be $\sim$10 to 12 mm, a little larger than that experimentally deduced in Ref. [37], i.e., $\sim$9 mm in diameter for a ^{17}F beam. The beam-purity optimization was achieved by recording the energy spectrum of the secondary beam at different Si detectors placed across the EXOTIC beam line. In Fig. 1, the energy spectrum of the secondary beam can be seen as recorded from the end-channel Si detector placed at the target ladder. The purity of the secondary beam was at maximum 44% to minimum 31%, depending on the simultaneous presence of the contaminant ^{7}Be^{4+} [$\sim$20%, produced via the reaction ^{3}He(^{6}Li,^{7}Be)d] and ^{6}Li^{3+} scattered primary beam (18%). A beam of ^{3}He was collected, as a byproduct of elastic scattering in the primary gas target at a level of 34% to 43% purity. For most of the runs the ^{7}Be contaminant beam was reduced below 1% with an appropriate handling of both the 30° bending magnet and the Wien filter. The transmission of the facility was smaller than the original value (1.35 %) quoted in Ref. [38] due to improvements on the beam optics and beam profiling achieved by adding extra collimator sets and the two PPAC detectors.

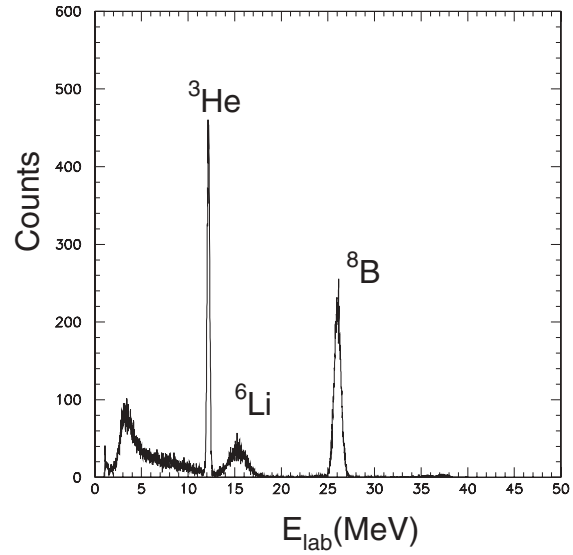

FIG. 1. A typical beam spectrum obtained in a beam monitor at the target ladder.

B. Experimental setup

A schematic layout of our setup is presented in Fig. 2. All the incident beam particles are going through two PPAC detectors, positioned before and after the entrance of the beam in the chamber, and are stopped in a Si three-stage telescope set at zero degrees ($E_1 \sim 45$ μm, $E_2 \sim 45$ μm, $E \sim 2000$ μm), which is used both as a target and as a detector. The beam is stopped before the third stage of the telescope. A coincidence requirement is applied between PPAC$_A$, PPAC$_B$, and the OR of the three stages of the telescope. Times of flight(TOF) are recorded between PPAC$_A$ as well as between PPAC$_B$ and the three stages of the silicon telescope. The first TOF was utilized for reaction and projectile discrimination, while the latter for scattering event rejection as well as spurious event rejection due to the implantation of the radioactive projectile. ^{8}B nuclei with a half-life of 750 ms beta-decay to ^{8}Be which is populated mainly to its first excited state at $\sim$3 MeV and which finally decays to two alpha particles. Home-made preamplifiers coupled with the low-resistivity thin silicon parts of the telescope allowed a time resolution in our system of the order of 2 ns (FWHM for a TOF between PPAC$_A$

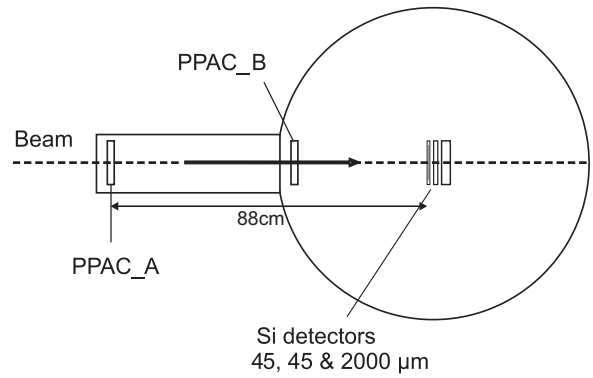

FIG. 2. A schematic setup of the ^{8}B + ^{28}Si fusion experiment.

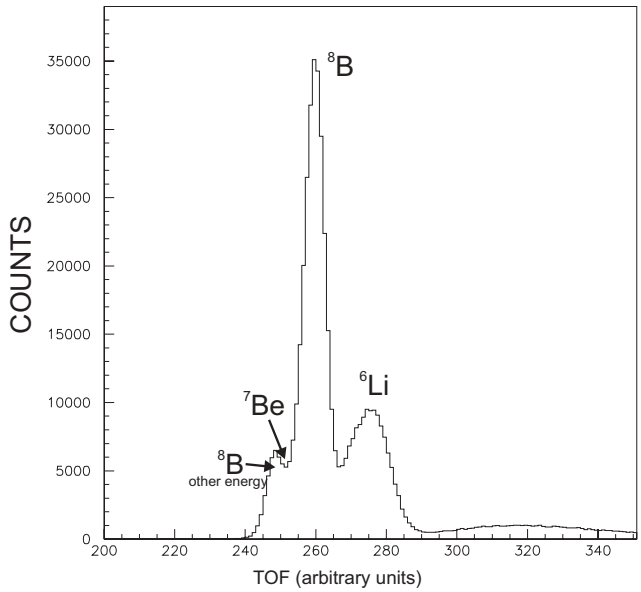

FIG. 3. A typical TOF spectrum obtained in the reaction ^{8}B + ^{28}Si. The main peak corresponds to the ^{8}B beam at 35 MeV. The boron beam projectiles cover the distance between PPAC$_A$ to $E1$ in 58 ns.

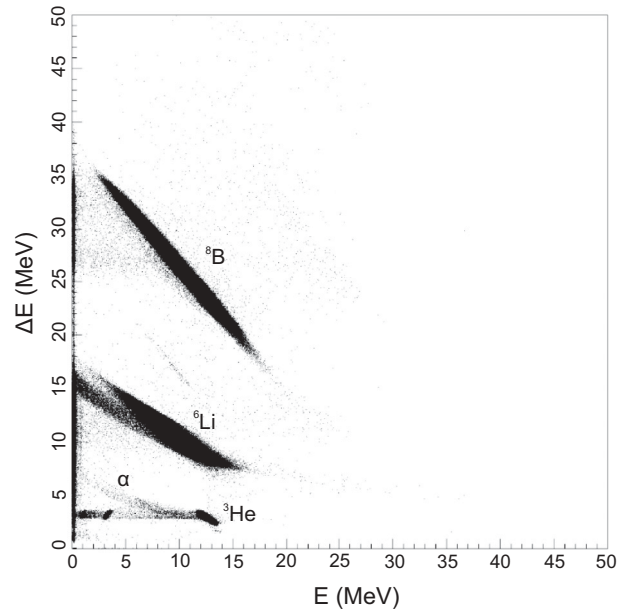

FIG. 4. A typical two-dimensional spectrum between the energy in the first silicon detector, $E1$, vs the deposited energy in the sum of the other two detectors, $E2 + E3$.

and first stage of the telescope). A typical spectrum appears in Fig. 3. Special care was taken for pileup rejection. We have obtained pileup rejection between two time-contiguous boron pulses and alpha-particle pulses from the boron decay with resolving time less than the pulse rising time, that is, 15 ns. Our techniques will be comprehensively presented in a forthcoming paper, while some relevant points will be described below.

In a first approach, similar to one applied in Ref. [35], the preamplifier signal was fed to a timing filter amplifier (TFA) with output pulse rise time of 20 ns and subsequently to a single constant fraction. The same signal was used to create the delayed START and the STOP signal in a conventional time-to-amplitude converter (TAC). Comparison of the energy spectrum with this timing spectrum allowed us to reject pileup events in the timing range of 50 ns to 5 μs. In a second approach by using a home-made constant-fraction discriminator [39] having two fractions of discriminations, one at 30% and the other at 80%, we were able to reject pileup events arriving even between 10 to 20 ns. Finally, in a third approach, the TFA signal was fed to a home-made fast stretcher (FS) module of the INFN Milano, used for the BaF2 signals [40], that gives two outputs: a slow and a fast one. The comparison of these two signals allowed a further reduction for pileup events arriving between 20 and 500 ns.

III. DATA REDUCTION AND ANALYSIS

For the determination of fusion cross sections we have been exploiting the fact, that during the collision of the proton drip nucleus ^{8}B with the silicon target, alpha particles are produced mainly via evaporation. Therefore for our data reduction, two-dimensional plots were formed for the alpha-particle identification $E1$ % $E2 + E3$ ($E1 \sim 45$ μm, $E2 \sim 45$ μm, $E3 \sim 2000$ μm). A typical spectrum is displayed in Fig. 4. Alphas were integrated with a contour in the bidimensional spectrum, a TOF window on boron projectiles, and a contour on the beam spot on the target. A small contamination in the TOF window of the boron beam from lithium projectiles was estimated to give only a ~0.25 % contribution on the produced alphas due to lithium collisions, while the contribution due to beryllium collisions was almost zero. Alphas were normalized to the boron beam particles, and evaporation reaction probabilities relevant to the alpha channels at each projectile energy E were formed as follows:

$$P(E') = \frac{N_\alpha}{N_{^8B-\text{beam}}}. \tag{1}$$

Alpha-evaporation integral cross sections were formed by the following formula:

$$\sigma_I(E') = \frac{m \ln[1 - P(E')] \times 10^{31}}{\rho N_A R_{\max}} \text{ mb}. \tag{2}$$

where m is the mass of the target in amu, $P(E)$ is the evaporation reaction probability, ρ is the density of the target material in gr/cm^3, N_A is the Avogadro number, and $R_{\max}$ is the range of boron particles in the target material in μm. The above quantity measured with this method is an energy-integrated cross section which is related to the alpha-evaporation cross section, σ_α, via the relation

$$\sigma_I(E') = \frac{\int_0^{E'} \sigma_\alpha(E)(dR/dE)dE}{\int_0^{R_{\max}} dR}. \tag{3}$$

The α evaporation cross sections $\sigma_\alpha(E)$ can be unfolded from the above relation via recursion relations as explained in Ref. [34]. Our results are included in Table I and are compared with CASCADE calculations [41], displaying a very

TABLE I. Measured alpha-production cross sections for $^{8}B + ^{28}Si$, $\sigma_{\alpha}^{meas.}$, are compared with cascade calculations, $\sigma_{\alpha}^{cascade}$. Assigned errors include a statistical uncertainty and an uncertainty due the probability fits. R is the ratio of proton channels vs alpha channels in the evaporation procedure, as estimated from cascade calculations. Finally in last column appear the complete fusion cross sections, $\sigma_{CF}^{meas.}$ determined in this work, taking into account this ratio.

E_{lab} (MeV)	$\sigma_{\alpha}^{meas.}$ (mb)	$\sigma_{\alpha}^{cascade}$ (mb)	R (%)	$\sigma_{CF}^{meas.}$
35	780 ± 28	741	20	940 ± 36
30	557 ± 21	531	63	864 ± 34
25	395 ± 18	454	68	761 ± 30
20	322 ± 13	291	90	553 ± 22

good agreement with them. This justifies an estimation of the proton multiplicity in the same evaporation context. The estimated ratios of proton channels to alpha channels are also included in Table I, and finally the experimental fusion cross section are presented in the same table and displayed in Fig. 5. It is expected that in this measurement the observed alphas are coming under an evaporation process related to complete fusion, but not excluding the part of evaporation of a compound created by the fragment of boron, ^{7}Be, with silicon. This last part corresponding to incomplete fusion is estimated via the breakup kinematics and cascade calculations to account only for 6% of the total fusion cross section. Therefore the present results could be taken to be closer to total fusion cross sections. It should be noted here that by total fusion we mean the sum of complete and incomplete fusion, by complete fusion we mean the fusion of the whole projectile and the taget nuclei, and by incomplete fusion we mean the partial fusion of one part of the projectile and the target nucleus

The α -production results are compared in Fig. 6 with previous data obtained mainly from ^{6}Li and ^{7}Li projectiles on various targets, and a few results of ^{6}He on ^{209}Bi and ^{64}Zn, as appear in Refs. [42,43]. The remarkable fact that all data points, except the ones originating from ^{6}He, fall upon

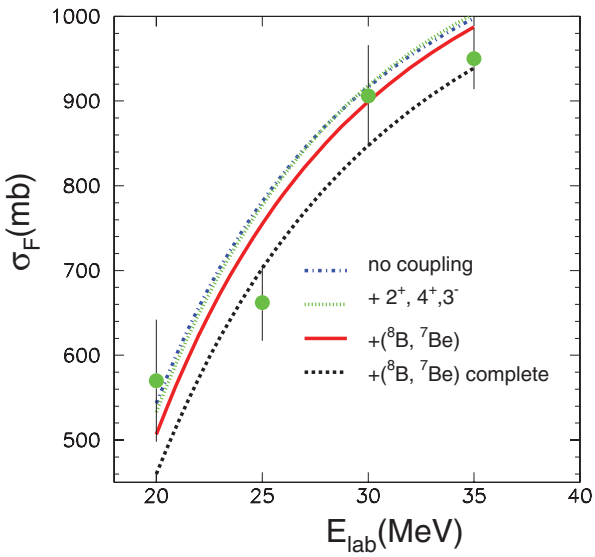

FIG. 5. (Color online) Present fusion cross sections are compared with coupled-channel calculations.

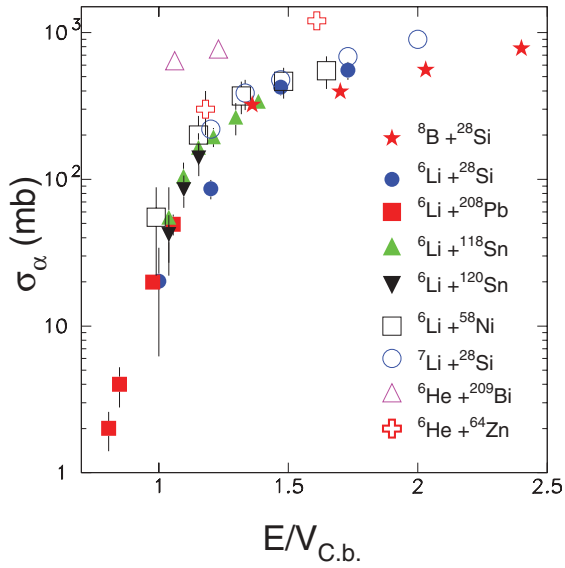

FIG. 6. (Color online) α-production cross sections due to fusion of $^{8}B + ^{28}Si$ are designated with stars. Present results are compared with previous data of α production of ^{6,7}Li and ^{6}He on various targets. The figure has been reproduced from Refs. [42,43], where the previous results were taken from Refs. [16,44–47].

the same universal curve was underlined in Ref. [42]. Even more interesting is that the present results, designated with solid stars, follow the trend of the universal curve but in a reduction of the order of ∼20%; this is well understood, as the boron particles are the only projectiles in this curve that do not produce alpha particles in a breakup process but only in a fusion process.

IV. COUPLED-CHANNEL CALCULATIONS

Coupled reaction channels (CRC) calculations were performed using the code FRESCO [48]. Inelastic excitations of the 1.78 MeV 2^{+}, 4.62 MeV 4^{+}, and 6.87 MeV 3^{-} states of ^{28}Si were included. The $B(E\lambda)$ values were taken from Refs. [49–51] for $\lambda = 2, 3$, and 4, respectively. The real nuclear potential was obtained using the double-folding model and the M3Y interaction, with nuclear matter densities obtained from Ref. [52] for ^{8}B and derived from the nuclear charge density of Ref. [53] by unfolding the proton charge distribution and making the isoscalar assumption, $\rho_N = 1 + (N/Z)\rho_p$, for ^{28}Si. The imaginary potential was of "interior" Woods-Saxon form with parameters $W = 50$ MeV, $R_w = 1.00 \times (A_p^{1/3} + A_t^{1/3})$ fm, and $a_w = 0.3$ fm to simulate the ingoing-wave boundary condition. Nuclear transition potentials were also calculated using the double-folding procedure with Tassie model transition densities [54] defined as

$$g(r) = \frac{d\rho_N(r)}{dr} \tag{4}$$

and normalized such that

$$M_N = \int_0^{\infty} g(r) r^{L+2} dr, \tag{5}$$

TABLE II. States in ^{29}P coupled to in the CRC calculations.

E_x (MeV)	J^π
0.00	$1/2^+$
1.38	$3/2^+$
1.95	$5/2^+$
3.45	$7/2^-$
4.34	$3/2^-$

where, for nuclei with ground-state spin-parity 0^+, M_N is the *nuclear* reduced matrix element, given by $M_N = (1 + N/Z)M_p$ and $M_p = \sqrt{B(E\lambda)}$, again making the isoscalar assumption. All double-folding potentials were calculated with the code DFPOT [55].

Single-proton stripping to the $3/2^-$ ground and $1/2^-$ first excited states of ^{7}Be and the ^{29}P states given in Table II was also included.

The $\langle ^{8}\mathrm{B}|^{7}\mathrm{Be} + p\rangle$ form factors were taken from Ref. [56] while the $\langle ^{29}\mathrm{P}|^{28}\mathrm{Si} + p\rangle$ form factors were taken from Ref. [57]. The exit partition potential was again of double-folded real plus interior Woods-Saxon form, the ^{7}Be density being taken from Ref. [52] and the ^{29}P density calculated using the liquid-drop model of Ref. [58]. Ground-state reorientation and coupling to the $1/2^-$ first excited state of ^{7}Be were also included, taking the $B(E2)$ value from Ref. [59] and again using double-folded nuclear transition potentials making the isoscalar assumption.

The results are compared with the data in Fig. 5. It is seen that the inelastic couplings leave almost unaffected the one-barrier calculation, while couplings to one-proton transfer are suitable for reducing the cross section closer to the data. This reduction is only in the range of 2% to 5% depending on the energy. As the uncertainty assigned to the data is large and the incomplete fusion part was not disentangled in this measurement, it is not useful to make any further discussion on the subject. Moreover, as was found in Ref. [9], total fusion cross sections for weakly bound systems are not affected by the breakup process at energies above the Coulomb barrier.

V. COMPARISONS WITH OTHER WEAKLY BOUND PROJECTILES

To answer the general question, what is the difference in the fusion cross section produced by weakly bound but stable projectiles and drip-line ones, neutron rich or proton rich, we will try in the following to benefit from comparisons of different projectiles on various targets. Comparison will be made between ^{6}Li, ^{7}Li, ^{6,8}He, ^{7,9}Be, and various targets: ^{28}Si, ^{27}Al, ^{60}Zn, ^{208}Pb, ^{209}Bi, and ^{238}U. Comparisons will be also made with the previous data on ^{8}B + ^{58}Ni. A fair comparison has to exclude at least the static effects between the various projectiles and targets, taking into account variations for the radii R_B, barrier heights V_B, and also the thickness of the barrier closely related to the curvature, $\hbar\omega$. All these components are directly affecting the tunneling probability. To take into account all these parameters we decided to use the prescription described in Ref. [60], which is originated by the Wong model. In that respect the comparison is susceptible to the limitations of this model; however, in the following we will show the advantage of using this prescription. In this comparison we also took care to do comparisons between similar types of fusion cross sections. Therefore we have grouped the measurements in three categories: total, complete, and "complete to total" fusion cross sections. The "complete to total" fusion cross sections refer mainly to complete fusion cross sections where the incomplete part was not disentangled from the complete part, and therefore some mixing may occur. The present fusion cross sections belong to this last category and, since incomplete fusion is estimated to be small, they can be considered to be "almost" total fusion cross sections.

Wong obtained for the fusion cross section the following analytic expression, approximating the barrier by a parabola (an inverted harmonic oscillator potential) and neglecting the variation of the barrier radius with angular momentum:

$$\sigma_F^W = R_B^2 \frac{\hbar\omega}{2E_{\mathrm{c.m.}}} \ln\left[1 + \exp\left(\frac{2\pi(E_{\mathrm{c.m.}} - V_B)}{\hbar\omega}\right)\right]. \quad (6)$$

Into this scheme the fusion cross sections σ_F and the energy $E_{\mathrm{c.m.}}$ of the projectile can be reduced by using the following formulas:

$$\sigma_F \rightarrow F(x) = \frac{2E_{\mathrm{c.m.}}}{\hbar\omega R_B^2}\sigma_F, \quad (7)$$

corresponding to an energy $E_{\mathrm{c.m.}}$ of the projectile reduced to the quantity x given by the equation

$$E_{\mathrm{c.m.}} \rightarrow x = \frac{E_{\mathrm{c.m.}} - V_B}{\hbar\omega}. \quad (8)$$

Fusion functions $F(x)$ as a function of x were determined for all data via the above relations. Curvatures ($\hbar\omega$), radii (R_B), and potential heights (V_B) were deduced by using the Christensen-Winther potential [61], and the obtained values are included in Table III. The reduced fusion cross sections

TABLE III. The potential height, radius, and curvature for various sytems considered in this work, taking into account a Christensen potential [61].

Reaction	R_B (fm)	V_B (MeV)	$\hbar\omega$
^{8}B + ^{28}Si	7.935	11.67	3.662
^{8}B + ^{58}Ni	8.772	21.258	4.38
^{6}Li + ^{28}Si	7.932	7.008	3.223
^{6}Li + ^{90}Zr	11.477	18.703	3.521
^{6}Li + ^{209}Bi	11.04	30.534	5.148
^{9}Be + ^{27}Al	8.269	8.353	2.955
^{9}Be + ^{209}Bi	11.364	39.131	4.7
^{9}Be + ^{208}Pb	11.351	39.173	4.704
^{10}Be + ^{209}Bi	11.483	39.227	4.456
^{11}Be + ^{209}Bi	11.6	38.857	4.226
^{4}He + ^{197}Au	10.66	20.032	5.219
^{6}He + ^{64}Zn	9.194	8.742	3.197
^{6}He + ^{197}Au	11.127	19.25	4.147
^{6}He + ^{238}U	11.55	21.65	4.284
^{6}He + ^{209}Bi	11.259	19.761	4.171
^{8}He + ^{197}Au	11.477	18.703	3.521

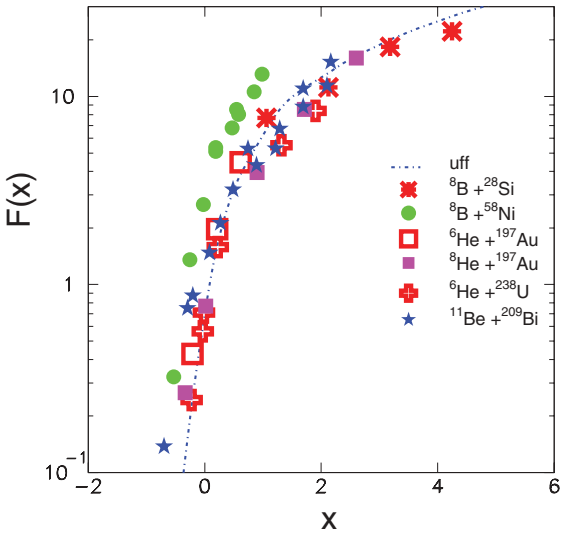

FIG. 7. (Color online) "Complete to total" fusion functions, calculated via relations (1)–(3) and the parameters included in Table III, for various projectiles and targets, are compared with the present data on ^{8}B + ^{28}Si, and the universal function, uff, designated with the dotted-dashed line. The previous data are taken from ^{8}B + ^{58}Ni [19], ^{6,7}He + ^{197}Au [18], ^{6}He + ^{238}U [15], ^{6}He + ^{64}Zn [16], and ^{11}Be + ^{209}Bi [14]. It should be noted that the adopted fusion cross sections in this comparison are considered in the literature as complete fusion cross sections, but the incomplete part was not measured. Therefore they may include a small incomplete fusion part.

for selected systems studied previously and the present results are compared in Figs. 7, 8, and 9 together with the universal fusion function (uff) defined also in Ref. [60] via the relation

$$F_0(x) = \ln[1 + \exp(2\pi x)]. \tag{9}$$

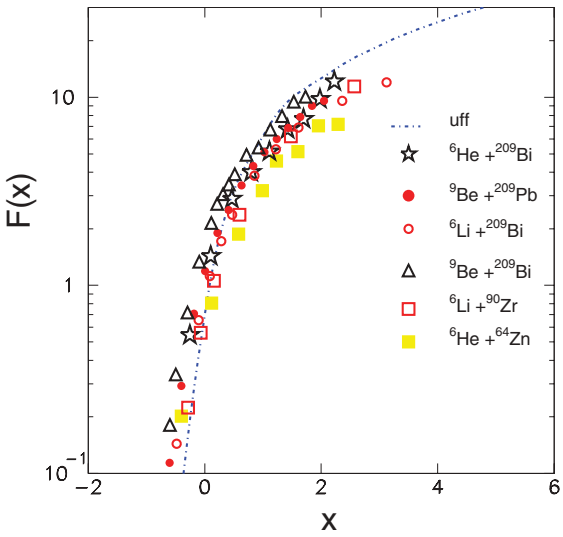

FIG. 8. (Color online) Complete fusion functions, calculated via relations (1)–(3) and the parameters included in Table III, for various projectiles and targets, are compared with the universal function, uff, designated with the dotted-dashed line. The previous data are taken from ^{6}He + ^{209}Bi [13], ^{9}Be + ^{208}Pb [64], ^{9}Be + ^{209}Bi [14], ^{6}Li + ^{209}Bi [64], and ^{6}Li + ^{90}Zr [66].

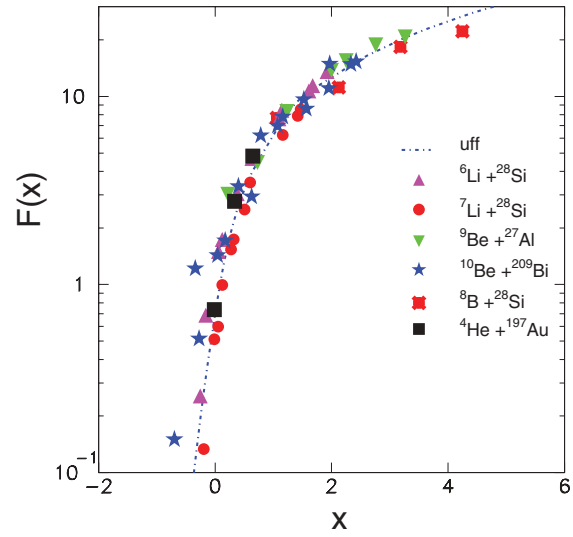

FIG. 9. (Color online) Total fusion functions, calculated via relations (1)–(3) and the parameters included in Table III, for various projectiles and targets, are compared with the universal function, uff, designated with the dotted-dashed line. The previous data are taken from ^{6,7}Li + ^{28}Si [63], ^{9}Be + ^{27}Al [65], and ^{10}Li + ^{209}Bi [14].

It is obvious that, in principle, all data obtained with stable or radioactive weakly bound projectiles follow the same trend of the uff curve and only occasionally present large deviations, possibly due to the measurement uncertainties. A part of these deviations should be related to dynamical effects such as couplings to continuum and/or to transfer, as comprehensively explained by Gomes *et al.* in Ref. [62]. At the higher energy part, the complete fusion data, Fig. 8, as well as to some extent the "complete to total" fusion data, Fig. 7, present the standard suppression due to the missing incomplete fusion part. On the other hand, the total fusion results, Fig. 9, are very compatible with the uff one-barrier penetration calculation.

Further on, our results are not compatible with previous results on ^{8}B + ^{58}Ni in the overlapping energy region and therefore to a large fusion radius, such as the ones reported for the nickel target. Of course, this conclusion is susceptible to any problems originating from the type of comparison. The large cross sections obtained in the ^{8}B + ^{58}Ni fusion reaction below and above the barrier have been explained in Ref [19] via a model based on an angular momentum limit. However, the differences seen between the two targets are not straightforward, and this fact needs further investigation.

As a general comment we can point out the remarkable fact that most of the data for, e.g., ^{6}He + ^{238}U [15], ^{6}He + ^{209}Bi [13], and ^{6,8}He + ^{197}Au [18], present excellent compatibility with results of weakly bound but stable projectiles such as ^{6}Li + ^{28}Si [63], ^{6,7}Li + ^{209}Bi [64], ^{9}Be + ^{208}Pb [64], and ^{9}Be + ^{27}Al [65], well bound stable projectiles such as ^{4}He + ^{197}Au [18], and the present results of a proton drip-line projectile and the universal curve in a BPM formalism. Only some of the data scatter above and below the uff curve, creating a deviation band of 60%. These deviations need further investigation, as they may have been caused by special features of the measurements. For

all data, small deviations between the data and the uff curve could be attributed to coupled-channel effects [60,62]. In the present study, preliminary coupled-channel calculations, e.g., one-proton transfer couplings, predict small deviations of the order of 2% to 6%. The large error of the data, however, does not allow further speculation on this subject.

VI. SUMMARY AND CONCLUSIONS

We have measured alpha production cross sections for the system ^{8}B + ^{28}Si by means of an active target technique, and subsequently obtained fusion cross sections at near barrier energies with the aid of CASCADE calculations. These results were compared with previous fusion data obtained by various weakly bound neutron-rich light projectiles, either stable or radioactive ones, after they were appropriately reduced in energy and cross section [60]. The reduction was based on a potential, obtained in a systematic fit by Christensen and Winther [61]. The results indicate the following outstanding conclusions.

Despite its proton halo nature, ^{8}B fuses with ^{28}Si at near-barrier energies, in the same way as other weakly bound but stable projectiles on the same or similar targets, following, in principle, fusion of two nuclei, described by one-barrier penetration tunneling. Small deviations are due to coupling channel effects. It is remarkable that the same conclusions can be drawn from the comparison of fusion cross sections obtained by various neutron-rich stable and exotic light nuclei with various medium or heavy targets. As was suggested in Refs. [15,63] and recently supported in [17,18], if the transfer channel is properly subtracted and if, for comparison purposes, reduced cross sections and energies are deduced properly [17], then the above conclusion may be general for all light weakly bound projectiles.

ACKNOWLEDGMENTS

We would like to warmly acknowledge Nick Keeley for useful discussions and theoretical support of this work. The research leading to these results has received funding from the European Union Seventh Framework Programme FP7/2007-2013 under Grant Agreement No. 262010-ENSAR. This work was partially supported by the Italian MIUR within the project RBFR08P1W2_001 (FIRB 2008).

[1] A. B. Balantekin and N. Takigawa, Rev. Mod. Phys. **70**, 77 (1998).
[2] C. Y. Wong, Phys. Rev. Lett. **31**, 766 (1973).
[3] R. G. Stokstad and Y. Eisen, S. Kaplanis, D. Pelte, U. Smilansky, and I. Tserruya, Phys. Rev. Lett. **41**, 465 (1978).
[4] M. Beckerman *et al.*, Phys. Rev. Lett. **45**, 1472 (1980).
[5] C. H. Dasso, S. Landowne, A. Winther, Nucl. Phys. A **405**, 381 (1983).
[6] D. Castro-Rizzo and N. Alamanos, Nucl. Phys. **443**, 525 (1985).
[7] L. F. Canto, P. R. S. Gomes, R. Donangelo, and M. S. Hussein, Phys. Rep. **424**, 1 (2006).
[8] N. Keeley, R. Raabe, N. Alamanos, and J. L. Sida, Prog. Part. Phys. **59**, 579 (2007).
[9] P. R. S. Gomes *et al.*, Phys. Rev. C **71**, 034608 (2005).
[10] A. Gomez and E. F. Aguilera, Nucl. Phys. A **735**, 425 (2004).
[11] V. Jha and S. Kailas, Phys. Rev. C **80**, 034607 (2009).
[12] A. Yoshida *et al.*, Phys. lett. B **389**, 457 (1996)
[13] J. J. Kolata *et al.*, Phys. Rev. Lett. **81**, 4580 (1998).
[14] C. Signorini *et al.*, Nucl. Phys. A **735**, 329 (2004).
[15] R. Raabe *et al.*, Nature (London) **431**, 823 (2004).
[16] V. Scuderi *et al.*, Phys. Rev C **84**, 064604 (2011)
[17] A. Di Pietro *et al.*, Phys. Rev. C **69**, 044613 (2004).
[18] A. Lemasson *et al.*, Phys. Rev. Lett. **103**, 232701 (2009).
[19] E. F. Aguilera and J. J. Kolata, Phys. Rev C **85**, 014603 (2012).
[20] C. A. Bertulani, Phys. Rev. C **49**, 2688 (1994).
[21] J. von Schwarzenberg, J. J. Kolata, D. Peterson, P. Santi, M. Belbot, and J. D. Hinnefeld, Phys. Rev. C **53**, R2598 (1996).
[22] H. Esbensen, G. F. Bertsch, and K. A. Snover, Phys. Rev. Lett. **94**, 042502 (2005)
[23] F. Schumann *et al.*, Phys. Rev. C **73**, 015806 (2006).
[24] V. Guimaraes *et al.*, Phys. Rev. Lett. **84**, 1862 (2000).
[25] E. F. Aguilera *et al.*, Phes. Rev. C **79**, 021601(R) (2009).
[26] R. E. Warner, C. P. Browne, S. E. Darden, J. J. Kolata, A. Rollefson, P. A. Kimoto, and A. Galonsky, Phys. Rev. C **37**, 1884 (1988).
[27] R. E. Warner, A. M. Van den Berg, K. M. Berland *et al.*, Phys. Rev **40**, 2473 (1989).
[28] R. E. Warner, K. M. Berland, W. F. Rulla *et al.*, Nucl. Phys. A **516**, 416 (1990).
[29] A. C. C. Villari, W. Mittig, E. Plagnol *et al.*, Phys. Lett. B **268**, 345 (1991).
[30] I. Licot, N. Added, N. Carlin, G. M. Crawley, S. Danczyk, J. Finck, D. Hirata, H. Laurent, D. J. Morrissey, M. M. deMoura, H. R. Schelin, J. Stasko, M. Steiner, A. A. P. Suaide, A. Szanto de Toledo, E. M. Szanto, M. Thoennessen, and J. A. Winger, Phys. Rev. C **56**, 250 (1997).
[31] W. Mittig, J. M. Chouvel, and Zhan Wen Long *et al.*, Phys. Rev Lett. **59**, 1889 (1987).
[32] A. Gillibert, L. Bianci, A. Cunsolo *et al.*, Phys. Lett. B **176**, 317 (1986).
[33] R. E. Warner, R. A. Patty, P. M. Voyles *et al.*, Phys. Rev C **54**, 1700 (1996).
[34] A. Pakou, A. Musumarra, D. Pierroutsakou *et al.*, Nucl. Phys. A **784**, 13 (2008).
[35] A. Musumarra, P. Figuera, F. De Luca *et al.*, Nucl. Instrum. Methods B **612**, 399 (2010).
[36] F. Farinon *et al.*, Nucl. Instrum. Methods B **266**, 4097 (2008).
[37] M. Mazzocco *et al.*, Phys. Rev. C **82**, 054604 (2010).
[38] M. Mazzocco *et al.*, Nucl. Instrum. Meth. B. **266**, 4665 (2008).
[39] R. Bassini *et al.*, IEEE Nuc. Sci. Symp. Conf. Rec. (2006), doi: 10.1109/NSSMIC.2006.356206.
[40] C. Boiano *et al.*, IEEE Nucl. Sci. Symp. Conf. Rec. (2004), doi: 10.1109/NSSMIC.2004.1462491.
[41] F. Puhlhofer, Nucl. Phys. A **280**, 267 (1979).
[42] A. Pakou, N. Alamanos, A. Gillibert *et al.*, Phys. Rev. Lett. **90**, 202701 (2003).
[43] A. Pakou, N. G. Nicolis, K. Rusek *et al.*, Phys. Rev. C **71**, 064602 (2005).
[44] N. Keeley *et al.*, Nucl. Phys. A **571**, 326 (1994).

[45] K. O. Pfeiffer, E. Speth, and K. Bethge, Nucl. Phys. A **206**, 545 (1973).
[46] E. F. Aguilera *et al.*, Phys. Rev. lett. **84**, 5058 (2000).
[47] R. Raabe *et al.*, Phys. Rev. C **74**, 044606 (2006).
[48] I. J. Thompson, Comput. Phys. Rep. **7**, 167 (1988).
[49] S. Raman, C. W. Nestor, Jr., and P. Tikkanen, At. Data Nucl. Data Tables **78**, 1 (2001).
[50] T. Kibédi and R. H. Spear, At. Data Nucl. Data Tables **80**, 35 (2001).
[51] B. A. Brown, W. Chung, and B. H. Wildenthal, Phys. Rev. C **21**, 2600 (1980).
[52] A. Bhagwat, Y. K. Gambhir, and S. H. Patil, Eur. Phys. J. A **8**, 511 (2000).
[53] S. W. Brain, A. Johnston, W. A. Gillespie, E. W. Lees, and R. P. Singhal, J. Phys. G **3**, 821 (1977).
[54] L. J. Tassie, Aust. J. Phys. **9**, 407 (1956).
[55] J. Cook, Comput. Phys. Commun. **25**, 125 (1982).
[56] P. Navrátil, C. A. Bertulani, and E. Caurier, Phys. Lett. B **634**, 191 (2006).
[57] A. Djaloeis, S. Gopal, J. Bojowald, W. Oelert, P. Turek, and C. Mayer-Böricke, Phys. Rev. C **28**, 561 (1983).
[58] W. D. Myers, Nucl. Phys. A **145**, 387 (1970).
[59] B. Buck and A. C. Merchant, J. Phys. G **14**, L211 (1988).
[60] L. F. Canto, P. R. S. Gomes, J. Lubian, L. C. Chamon, and E. Crema, Nucl. Phys. A **821**, 51 (2009).
[61] P. R. Christensen and A. Winther, Phys. Lett. B **65**, 19 (1976).
[62] P. R. S. Gomes, D. R. Otomar, T. Correa *et al.*, J. Phys. G: Nucl. Phys. **39**, 115103 (2012).
[63] A. Pakou *et al.*, Eur. Phys. J. A **39**, 187 (2009).
[64] M. Dasgupta *et al.*, Phys. Rev. C **70**, 024606 (2004).
[65] G. V. Marti *et al.*, Phys. Rev C **71**, 027602 (2005).
[66] H. Kumawat *et al.*, Phys. Rev. C **86**, 024607 (2012).